

Modelling probability of rainfall-induced shallow landslides in a changing climate, Otta, Central Norway

Caterina Melchiorre · Paolo Frattini

Received: 26 July 2010 / Accepted: 9 October 2011 / Published online: 10 December 2011
© Springer Science+Business Media B.V. 2011

Abstract We analyse slope stability conditions for shallow landslides under an extreme precipitation regime with regard to present and future scenarios, in order to first study the effect of changes in precipitation on stability conditions, considering uncertainty in the model parameters, and second to evaluate which factors contribute the most to model output and uncertainty. We used a coupled hydrological-stability model to study the hydrological control on shallow landslides in different precipitation regimes, with reference to the case study of Otta, located in central east Norway. We included a wide range of climatic settings, taking intensity, duration of the extreme events and two different antecedent precipitation conditions into account. Eleven future scenarios were determined using results of down-scaled meteorological models. Considering the uncertainty in the soil parameters, we used the Monte Carlo approach and probability of failure resulting from 5,000 trials was calculated for each precipitation scenario. In unstable areas the probabilities of failure at present and future conditions were compared using a bootstrapping method. Sensitivity analysis was carried out to understand how variations in input parameters influence the output of the selected model. The results show changes in the modelled stability conditions only if the effect of antecedent precipitation is not taken into account. The uncertainties in the predicted extreme precipitation events, soil parameters, and antecedent precipitation conditions do not allow any accurate estimation of changes in stability conditions for shallow landslides.

1 Introduction

Despite the small volume involved at the triggering of events, shallow landslides cause high numbers of fatalities and economic losses all over the world, due to their high frequency

C. Melchiorre (✉)

Department of Earth Sciences - Air, Water and Landscape Sciences, Uppsala University, Villavägen 16,
SE-752 36 Uppsala, Sweden
e-mail: caterina.melchiorre@geo.uu.se

P. Frattini

Department of Geological Sciences and Geotechnologies, University of Milano - Bicocca,
Piazza della Scienza 4, Milan 20126, Italy

and to the capacity of triggering devastating debris flows. Shallow landslides typically show a depth from a few decimetres to some meters, with a sliding surface located within the soil cover, frequently at the contact with the bedrock.

Meteo-climatic factors (i.e., intense rainfall, rapid snowmelt and antecedent rainfall) have a great influence in triggering shallow landslides. The study of climatic factors is important for understanding the hydrological response of soils and how climate change can influence shallow landslide initiation (Wieczorek and Glade 2005).

In the last decades several authors have intensively worked to understand the relationship between rainfall and landslides (Wieczorek and Glade 2005; Crosta and Frattini 2008). One of the main topics has been the definition of rainfall amount needed for landslide triggering, and several approaches have been used, both empirical (Crosta and Frattini 2001; Wieczorek and Glade 2005; Guzzetti et al. 2007) and physically based based (Wilson and Wieczorek 1995; Crosta 1998; Terlien 1998; Glade 2000; Frattini et al. 2009).

The recently published report of the Intergovernmental Panel on Climate Change (Solomon et al. 2007) points out, with high confidence, an on-going change in precipitation and temperature patterns. At high latitude, a general trend of increase in precipitation and temperature is estimated. Considering the high influence of climatic factors on landslide triggering and, consequently, on human lives and economy, it is crucial to study and evaluate the possible consequences of climate changes on landslide hazard.

The availability of climate scenarios based on General Circulation Models (GCM) and statistical downscaling techniques have posed new challenges to the scientific community in the evaluation of the effects of climate change on slope stability conditions. This problem has been addressed using two main types of approach. Some authors proposed statistical studies of landslides occurrences related to climatic factors in the recent past decades (Rebetz et al. 1997; Flageollet et al. 1999; Jomelli et al. 2004, 2007, 2009). Other authors used modelling approaches to estimate changes in stability conditions due to changes in climate, both at local (Dehn 1999; Dehn and Buma 1999; Dikau and Schrott 1999; Dehn et al. 2000; van Beek 2002; Schmidt and Glade 2003; Dixon and Brook 2007) and regional scale (Collison et al. 2000; Bathurst et al. 2005). However, none of these studies have addressed the effects of climate change in the Scandinavian region.

The present paper is part of a Norwegian research project called GeoExtreme (Jaedicke et al. 2008), aimed at studying the impact of climate changes on landslide hazard in the coming decades. The project focuses on the most common and destructive processes in Norway such as snow avalanches, earth flows, debris flows, and rock falls. Four areas were selected as case studies, according to climatic and landslide process conditions. One of these areas is Otta, located in central east Norway and mainly affected by rock falls and debris flows.

Since most of the debris flows in the study area are triggered as shallow slides (soil slip, Campbell 1974), we analysed the climatic control on shallow failures within the soil cover, by coupling a hydrological model to the one-dimensional infinite-slope stability analysis.

In this contribution we aim to:

- analyse the influence of present and future precipitations on the stability conditions of slopes;
- assess the effect of uncertainty when estimating slope stability conditions in future climate.

We have not taken the propagation of landslides into account, since the purpose of the paper is to characterize changes in triggering.

2 Methodologies

The main focus of the study is to evaluate changes in slope stability conditions due to climate change by using a coupled hydrological-stability model and climate scenarios.

In section 2.1 we first describe the climate scenarios, whereas the hydrological-stability model is presented in section 2.2.

In the modelling approach two main sources of uncertainty were considered: the first is related to the estimation of soil parameters and the second is related to climate modelling. We used results of 11 climatic models to simulate future climate and Monte Carlo simulations to model uncertainty of soil properties. For each climate scenario 5,000 Monte Carlo trials of the hydrological-stability model were executed, obtaining 5,000 maps of the Factor of Safety (FoS). Then we analysed which parameters contribute the most to uncertainty by means of variance-based Sensitivity Analysis (SA), as explained in section 2.3.

The results of Monte Carlo modelling were analysed by estimating the probability of failure P_f , defined as $P(\text{FoS} \leq 1)$. For each precipitation scenario a map of P_f was derived from the 5,000 maps of the FoS. In order to estimate the uncertainty of the P_f and its confidence interval, we used bootstrapping; a sampling procedure used in the estimation of data summaries. The bootstrapping method is discussed in section 2.4.

2.1 Extreme events and climate scenarios

The climate scenarios, provided by the GeoExtreme project (Jaedicke et al. 2008), are based on a dynamic regional climate modelling approach. In this approach a global model was first run with a resolution of 300 km. Its sea surface temperature output was then used as an input for a finer global atmospheric model with a 150 km resolution. Wind, temperature, and moisture data resulting from this model and the sea surface temperature data coming from the global model were then used as boundary conditions for a regional atmospheric model at 50 km resolution. As external forcing, the scenario A2 from the Special Report on Emission Scenarios (SRES) was used (Nakicenovic et al. 2000), which estimates a continuous increase of CO_2 until the year 2100. Three different intermediate models and eight different regional models (Sorteberg and Andersen 2008) were used to obtain a total of 11 scenarios of future climate. The results of this modelling phase are daily precipitations for a control period (1960–1990) and for a future scenario 2071–2100. Finally, the daily precipitations were bias-corrected according to historical precipitation records from the rain gauge in Otta. Within the Geo-Extreme Project (Asgeir Sorteberg, personal communication), the bias-correction was done in two steps to adjust both frequency and intensity of precipitation. The frequency of daily modelled rainfall was corrected by fitting a threshold value x_{mod} to truncate the empirical distribution of observed daily rainfall. The threshold was calculated from the empirical observed and modelled cumulative rainfall distribution as:

$$x_{mod} = F_{p,mod}^{-1}(F_{p,obs}(x_{obs})), \quad (1)$$

where F_p is the cumulative distribution function, F_p^{-1} its inverse, and x_{obs} is the minimum rainfall amount for a day to be considered wet and was set to 0.1 mm.

The second step was to calculate the cumulative distribution function for modelled and observed rainfall intensity, $F_{I, mod}$ and $F_{I, obs}$ respectively, by fitting a two-

parameter gamma distribution. The bias-corrected modelled rainfall $x'_{i,mod}$ was calculated as:

$$x'_{i,mod} = \begin{cases} F_{T,obs}^{-1}(F_{T,mod}(x_i)), & x_i > x_{mod} \\ 0, & x_i < x_{mod} \end{cases} \quad (2)$$

In order to estimate the return period of precipitation extremes for both present and future climate, we used the modified version (Førland 1987; Førland and Kristoffersen 1989) of the British M5-method (NERC 1975), as applied in Norway (Alexandersson et al. 2001). This method uses the Gumbel equation to estimate extreme precipitation with return period shorter or equal to 5 years, $P(5)$, whereas a semi-empirical equation, calibrated on Norwegian data, was applied to estimate extremes with return periods equal or longer than 5 years:

$$P(T) = P(5) * \exp(\lambda * \ln(T - 0.5) - 1.5), \quad (3)$$

where $P(5)$ is the precipitation with 5 year return period; T is the return period; $\lambda = 0.3584 - 0.0473 * \ln(P(5))$, if $25 < P(5) \leq 200$ as in Førland and Kristoffersen (1989).

2.2 Hydrological and stability model

In the last years several hydrological frameworks have been proposed for modelling hydrological conditions underlying shallow landslide initiation (Montgomery and Dietrich 1994; Iverson 2000; Borga et al. 2002; Wilkinson et al. 2002; Casadei et al. 2003; Rosso et al. 2006). These approaches differ for the conceptual model used to analyse the water content in the soil, varying from the relatively simple steady-state model based on topographic control of the subsurface flow (Montgomery and Dietrich 1994) to more complex ones, which simulate infiltration, evaporation, unsaturated and saturated flow, and storage (Wilkinson et al. 2002; Simoni et al. 2008).

The lack of detailed data on hydrological response of soil in the study area led us to choose models with a reduced number of parameters. We decided to test a combined version of the steady-state model (Montgomery and Dietrich 1994) and the infiltration model (Iverson 2000), as proposed in D'Odorico and Fagherazzi (2003) and D'Odorico et al. (2005). The use of the two models makes it possible to consider a wide variety of meteorological settings, as combinations of short and long-term precipitation.

2.2.1 Hydrological model

Water content in soils depends on precipitation at different time scales, with long-term precipitation controlling moisture content at the beginning of a storm and short-term precipitation contributing to raise the head pressure during a storm. The head pressure can be expressed as the result of the contribution of two components (D'Odorico et al. 2005):

$$\psi(t^*) = \psi_0 + \psi_1(t^*), \quad (4)$$

where ψ is the pressure head, ψ_0 is a long-term component produced by a long-term infiltration rate, and $\psi_1(t^*)$ is the short-term response to rainstorm.

In case of slope-parallel subsurface flow, ψ_0 increases linearly with the vertical saturated depth $h_z = Z-d_z$ (Iverson 2000):

$$\frac{\psi_0}{Z} = \left(1 - \frac{d_z}{Z}\right) \cos^2 \beta, \tag{5}$$

where Z is the soil depth in vertical direction, d_z is the vertical depth of the water table at the beginning of the storm, and β the slope angle.

If we assume parallel flow over an impermeable layer, and we focus our attention on ψ_0 at the contact of bedrock, it can be demonstrated (D’Odorico et al. 2005) that:

$$1 - \frac{d_z}{Z} = \frac{h}{H} = W, \tag{6}$$

where h represents the height of the water table, H the soil depth, both normal to the ground surface, and W the wetness index, ranging from zero to one (Beven and Kirkby 1979; Montgomery and Dietrich 1994). Hence, at the bedrock contact:

$$\frac{\psi_0}{Z} = W \cos^2 \beta. \tag{7}$$

In the topography-based steady-state approach (Montgomery and Dietrich 1994; D’Odorico et al. 2005) the wetness index can be expressed as:

$$W = \frac{q}{HK_s} \frac{A}{b \sin \beta}, \tag{8}$$

where q is the constant net recharge which is assumed to be equal to long-term precipitation, A the contributing area, K_s the hydraulic conductivity, b the width of the unit section, and $\frac{A}{b \sin \beta}$ the topographic index (Montgomery and Dietrich 1994). This equation of the steady flow model does not use any information regarding the duration of the net precipitation.

To characterize the triggering-landslide precipitation both in terms of intensity and duration, D’Odorico and Fagherazzi (2003) introduced the concentration time T_c , which is defined as the time necessary for the subsurface flow to travel from the most distant point in the drainage area to a selected point in the hollow. T_c is calculated as the ratio between the maximum length of drainage path and the specific discharge:

$$T_c = C \frac{\sqrt{A}}{K_s \sin \beta}, \tag{9}$$

where C is a dimensionless coefficient to account for factors such as soil heterogeneity and hollow shape that can influence the concentration time (D’Odorico and Fagherazzi 2003).

Thus, given a precipitation of defined duration T , we can estimate the partial contributing area A_p , equalling T_c with T in Eq. 9, as:

$$A_p = \left(\frac{T \times K_s \times \sin \beta}{C}\right)^2. \tag{10}$$

The second part of Eq. 4 is the short-term response to rainstorm (Iverson 2000). In case of soils close to saturation, this can be modelled by a reduced diffusive form of the Richards equation:

$$\frac{\partial \psi_1}{\partial t} = D_0 \cos^2 \beta \frac{\partial \psi_1^2}{\partial z^2}, \quad (11)$$

where D_0 is the maximum hydraulic diffusivity, which determines the transmission of pressure head in the soil profile. Solving this equation with appropriate boundary and initial conditions, the pressure head is calculated as (Iverson 2000):

$$\frac{\psi_1(t^*)}{Z} = \frac{I_z}{K_z} [R(t^*)] \quad \text{When } 0 \leq t^* \leq T^*, \quad (12)$$

$$\frac{\psi_1(t^*)}{Z} = \frac{I_z}{K_z} [R(t^*) - R(t^* - T^*)] \quad \text{When } t^* > T^*, \quad (13)$$

where I_z is the rate of rainfall event, t^* is the normalised time, T^* is the normalised duration of the precipitation, and R is the response function (Iverson 2000). These are defined as:

$$t^* = \frac{t}{Z^2/D}, \quad (14)$$

$$T^* = \frac{T}{Z^2/D}, \quad (15)$$

$$R(t^*) = \sqrt{t^*/\pi} \exp(-1/t^*) - \operatorname{erfc}(1/\sqrt{t^*}), \quad (16)$$

where D is equal to $4D_0 \cos^2 \beta$, t and T are the time in which the pressure head is calculated and the duration of precipitation.

2.2.2 Infinite-slope stability model

Considering that we are modelling the failure condition of shallow landslides, we adopted the infinite-slope stability model (Skempton and De Lory 1957), which is a good approximation of landslide geometry when the soil depth is small with respect to its length and width. The dimensionless FoS was calculated as (Iverson 2000):

$$FoS = \frac{\tan \phi}{\tan \beta} + \frac{c - \psi(Z, t) \gamma_w \tan \phi}{\gamma_s Z \sin \beta \cos \beta}, \quad (17)$$

where ϕ is the soil friction angle, c is the soil cohesion, γ_w and γ_s are the unit weight of water and soil, respectively.

2.3 Sensitivity Analysis

The aim of the SA is to quantify the effect of each input variable on the values of the final output model. Homma and Saltelli (1996) recognized two main types of SA. Global SA

focuses on the identification of key parameters whose uncertainty influences the output uncertainty the most. On the other hand, local SA emphasizes the key parameters with respect to the output itself and not to its uncertainty. We performed global SA using variance-based methods and local SA using graphical methods.

Variance-based methods have the advantages to cope with influence of scale and shape of the distribution of variables, to be quantitative, independent from assumption, and able to treat grouped factors (Saltelli 2002). The total variance V of the model output can be written as a sum of increasing dimensionality (Sobol 1993):

$$V = \sum_{i=1}^n V_i + \sum_{i=1}^n \sum_{\substack{j=1 \\ j \neq i}}^n V_{ij} + \dots, \quad (18)$$

where the first order terms V_i describe the contribution of each input parameter X_i to the total variance, the second order terms V_{ij} explain the contribution of the two-way parameter interaction (i.e., contribution of variable X_i on the variable X_j), and so on for the terms of increasing dimensionality. The term V_i represents the amount of variance that would be removed from the variance of the output, Y , in case we knew the true value of X_i . If we divide the term V_i by the total variance, we obtain the first order sensitivity index:

$$S_i = \frac{V_i}{V}. \quad (19)$$

The index S_i measures the relative importance of X_i in leading up the uncertainty. This index can be used to characterize which inputs influence the output uncertainty the most. This solves two related problems: to direct future research in reducing input uncertainty and to help researchers in selection of calibration variables. Considering the purpose of this contribution, the first aim is the most relevant. We treated correlated variables as group, using the approach suggested by Sobol (1993) and applied by Jacques et al. (2006).

Concerning local SA we applied a graphic method (Plate et al. 2000) to qualitatively investigate the effect of input variables on the hydrological-stability model. The graphical method uses modified scatter plots. The input variables are plotted on the x-axis and the variations (Δ_i) of the model output on the y-axis. The Δ_i values are calculated as variation of the model from an arbitrary baseline (b_i) to their original values. For each variable i the variation of the model output due to variation of i (Δ_i) was calculated as:

$$\Delta_i = Y(X) - Y(X_1, \dots, X_{i-1}, b_i, X_{i+1}, \dots, X_k), \quad (20)$$

where X is the vector of the k input variables and Y is the model output. By definition $\Delta_i=0$, when $X_i = b_i$.

Instead of plotting variations of model output as points, as in standard scatter plots, effects are plotted as segments, with slope equal to the partial derivative of the model output with respect to X_i . The visualization of the partial derivatives as segments allows the identification of trends and types of non-linear relationships between each input variable and the model output.

The plots contain information about:

- 1) the effect of input variables on the output: variables with no effect appear as horizontal lines;
- 2) the variable importance that is described by the overall vertical range;
- 3) the interaction with other variables that is described by the spread along the vertical range: variables with no interaction appear as a single line;
- 4) trends and non-linearity that are described by trends and non-linearity of derivatives.

2.4 Bootstrapping

Bootstrapping is a resampling method used in statistical inference to evaluate the accuracy of data summaries. The basic idea of the bootstrapping method is to use resampling to generate new data subsets, to fit the model in each subset, and then calculate model variability across the subsets. Depending on the distribution from which the new subsets are drawn, the bootstrapping is *non-parametric* or *parametric* (Davison and Hinkley 1997).

In this contribution *non-parametric bootstrapping* was used to calculate confidence intervals of the Pf. For each precipitation scenario, the 5,000 trials were randomly sampled with replacement for a significant number of trials, and for each subset the Pf is estimated. Finally, confidence intervals were calculated.

3 Study area

Otta is located in central southern Norway (Fig. 1) at the junction between the N–S trending Gudbrandsdalen valley and the E–W trending Ottadalen tributary valley. Both valleys have been glacially carved out through recurrent glaciations, and present steep valley sides are covered by glacial deposits. Exposed schists are heavily weathered and act as a source for soil development and rock falls. Rapid landslide (i.e., debris flows and rock falls) deposits at the bottom of many of the slopes covered by glacial and eluvial deposits demonstrate the high landslide activity during the Holocene.

The area has experienced channelized debris flow events (Cruden and Varnes 1996), mostly initiated as shallow slides within the soil cover (i.e., soil slips). Debris flow activity is testified by the presence of tracks and levees recognized during field activity, and through aerial photo interpretation. Debris flow processes affected Eastern Norway during most of

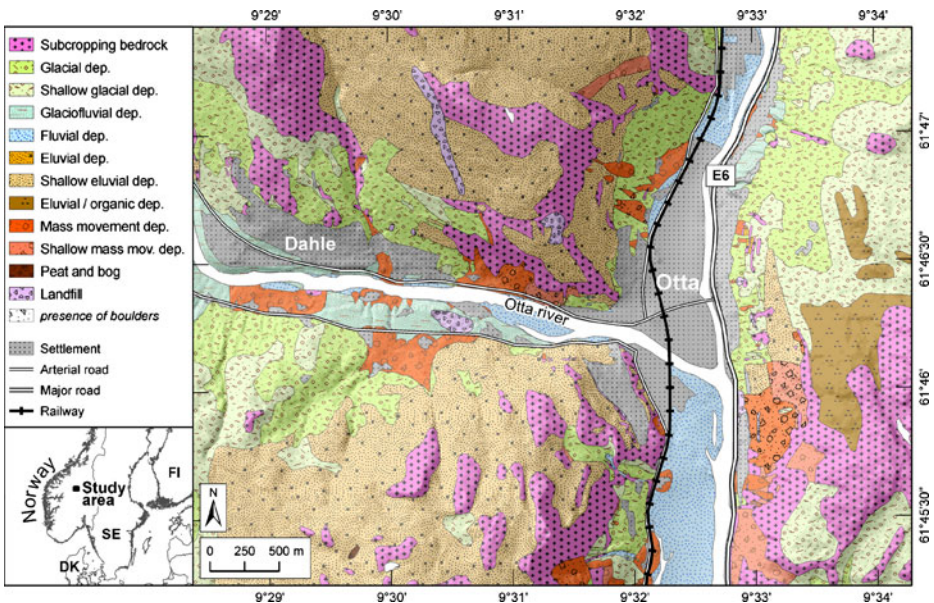


Fig. 1 Location map and Quaternary deposits map. The Quaternary deposits map is at scale 1:20,000 and 1:50,000 for the areas at low and high elevation, respectively

the Holocene, with alternation of relatively high and low activity (Sletten and Blikra 2007). Stratigraphy and chronological data show a lack of a clear relationship between regional climatic change and landslides. At the same time, this independency could evidence the temporal alternation of different weather conditions for triggering of debris flows. One interpretation can be that the main weather parameter inducing debris flow changed during the Holocene, meaning that in some periods intense rainfall and in some other periods intense solar radiation caused snow melting (Sletten and Blikra 2007).

Historical data demonstrate the importance of intense rainfall for triggering devastating debris flows. In 1789 the upper Gudbrandsdalen, where Otta is located, was affected by an extreme rainstorm causing the worst disaster ever recorded in eastern Norway, in terms of debris flows and flooding events. In 1938 an important debris flows and flooding event occurred in the Otta area, caused by 150 mm of precipitation in 3 days. More recently, in July 2006, an area around Garmo, 30 km eastern of Otta, experienced intense and localised precipitation that triggered six debris flows and some shallow landslides. In less the 1 h 150 mm of precipitation affected the area, corresponding to almost half of the yearly rainfall.

In May 2008 a debris flow event, triggered by a combined effect of rainfall and snow melt, caused considerable damage to some residential buildings and to the main road, fortunately without any deaths (Fig. 2).

Otta is a relatively dry area. Annual precipitation varied from a minimum of 303 mm/y to a maximum of 478 mm/y during the period 1971–1994. June, July, and August are the months with highest precipitation with average monthly rainfall above 50 mm. The maximum daily precipitation (i.e., 45 mm) was recorded in July.



Fig. 2 Example of a debris flow in Otta: (a) initiation of the debris flow as shallow slide in glacial deposits; (b) transport zone with channel erosion; (c) deposition zone with accumulation of debris and damages to human properties. The debris flow event was triggered in May 2008 by a combined effect of rainfall and snow melt. Photos courtesy of Kari Sletten

According to Sandersen et al. (1996) intensity-duration thresholds for debris flows can vary considerably in Norway, most likely due to the non-homogeneity of geological, geomorphologic, and climate settings. In a region with low precipitation, such as Otta, slopes have a lower precipitation threshold for initiating landslides than in regions affected by the highest rainfall events, since during the Holocene slopes have adjusted to climatic conditions. This makes it even more crucial to study the effect of climate change in a relatively dry region.

4 Analysis and results

4.1 Precipitation scenarios

Precipitation inputs for the hydrological-stability models were calculated at fixed return periods (i.e., 5, 50, 100, 500, and 1,000 years) and duration of 1 day, as described in section 2.1. Considering the importance of antecedent precipitations in defining pre-storm soil wetness conditions, we also calculated the intensity of extreme precipitation for extreme event following fixed valued of antecedent precipitation. This was achieved by filtering rainfall events according to fixed thresholds of antecedent precipitation (Frattini et al. 2009), thus removing precipitation peaks occurring in dry periods. We used two values of antecedent precipitation (15 and 30 mm) with duration of 4 days. The duration of 4 days was chosen based on the similarity of the deposits in Otta with the ones analysed by Frattini et al. (2009).

The calculation of the extreme events for the different return periods, both without and with filtering, was performed using data from: 1) rain gauge in Otta (1970–1995); 2) bias-corrected meteorological models run on the control period (1960–1990); 3) bias-corrected meteorological models run on the scenario period (2070–2100). The difference between the future and control scenario was scaled to the period 2011–2026 by using a linear function, as proposed in Sorteberg and Andersen (2008), and then added to the extreme event values calculated from historical rain gauge data to derive future scenarios.

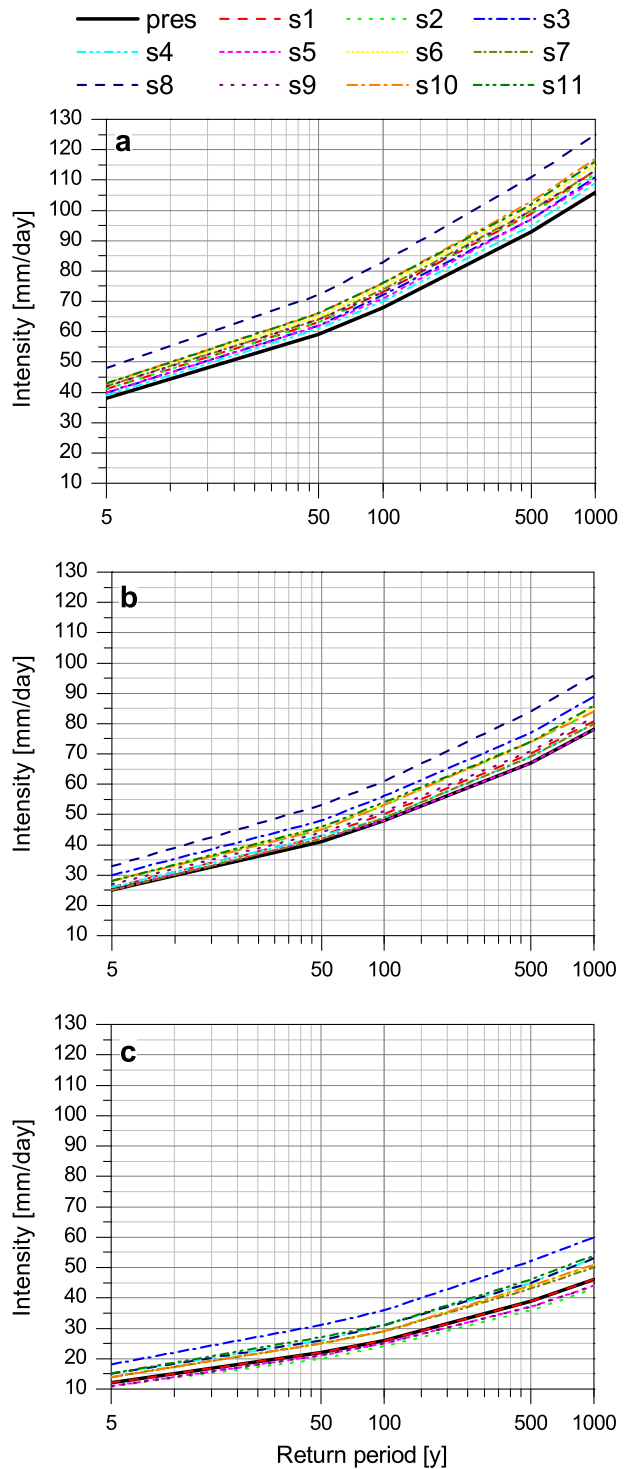
Figure 3 shows that the 11 climate models estimate a widely variable increase of extreme precipitation for the period 2011–2026, ranging from 2% to 26%. In percentage, the increase is higher for short return periods than for long return periods. Analysing the results for precipitations filtered with 15 mm in 4 days, we notice a spread of the future variation. With 30 mm threshold in 4 days we observe both decreasing and increasing of extreme events for the period 2011–2026. Moreover the maximum increase of precipitation considerably varies, moving from 26% in case of no-filtered precipitation to 46% in case of filtered precipitation.

4.2 Distributed physically based model–settings and validation

The coupled hydrological-stability model needs data of slope angle, intensity and duration of precipitation, and soil parameters (i.e., soil depth, soil unit weight, saturated hydraulic conductivity, diffusivity, cohesion, friction angle) to calculate FoS.

We derived a Digital Elevation Model (DEM) at 5 m cell resolution by interpolating 5 m interval contour lines with TOPOGRID tool in ArcGIS. From the DEM, we calculated the slope angle and the contributing areas by using the $D-\infty$ (Tarboton 1997) algorithm with RiverTool software.

Fig. 3 Precipitation intensity-frequency curves for present and the 11 future scenarios in case of antecedent precipitation equal to: 0 mm (a), 15 mm in 4 days (b) and 30 mm in 4 days (c)



To model the spatial distribution of the soil parameters we used a Quaternary deposits map (Fig. 1) compiled from two maps available at NGU (Norwegian Geological Survey) at 1:20,000 and 1:50,000 scale. The first includes all the areas from the valley floor to approximately 700 m a.s.l. These maps classify Quaternary deposits according to depth in two classes, below or above 1 m. Thanks to field surveys, we refined the soil depth

Table 1 Probability density function (pdf), mean (μ), and standard deviation (σ) for calibrated soil parameters used in the analysis

(a)							
Description	Soil depth [m]		K_s [m/s]		D_0 [m ² /s]		
	Normal pdf		Lognormal pdf		Lognormal pdf		
	μ	σ	μ	σ	μ	σ	
Glacial deposits	1.2	0.3	$1 \cdot 10^5$	$2.5 \cdot 10^6$	$4 \cdot 10^4$	$5 \cdot 10^5$	
Shallow glacial deposits	0.8	0.2	$1 \cdot 10^5$	$2.5 \cdot 10^6$	$4 \cdot 10^4$	$5 \cdot 10^5$	
Glaciofluvial deposits	1.2	0.3	$1 \cdot 10^4$	$2.5 \cdot 10^5$	$2 \cdot 10^3$	$2.5 \cdot 10^4$	
Fluvial deposits	4	0.6	$1 \cdot 10^3$	$2.5 \cdot 10^4$	$2 \cdot 10^2$	$3 \cdot 10^3$	
Eluvial deposits	1.2	0.3	$5 \cdot 10^5$	$1.5 \cdot 10^5$	$1 \cdot 10^3$	$1.25 \cdot 10^4$	
Shallow eluvial deposits	0.8	0.2	$5 \cdot 10^5$	$1.5 \cdot 10^5$	$1 \cdot 10^3$	$1.25 \cdot 10^4$	
Landslide deposits	1.2	0.3	$5 \cdot 10^5$	$1.5 \cdot 10^5$	$1 \cdot 10^3$	$1.25 \cdot 10^4$	
Landslide shallow deposits	0.8	0.2	$5 \cdot 10^5$	$1.5 \cdot 10^5$	$1 \cdot 10^3$	$1.25 \cdot 10^4$	
Peat and bog	2	0.5	$1 \cdot 10^6$	$2.5 \cdot 10^7$	$4 \cdot 10^5$	$5 \cdot 10^5$	
Eluvial deposits with high content of organic matter	0.8	0.2	$1 \cdot 10^6$	$2.5 \cdot 10^7$	$4 \cdot 10^5$	$5 \cdot 10^5$	
Landslide deposits with boulders	1.2	0.3	$2 \cdot 10^3$	$5 \cdot 10^4$	$5 \cdot 10^2$	$5 \cdot 10^3$	
Landslide shallow deposits with boulders	0.8	0.2	$2 \cdot 10^3$	$5 \cdot 10^4$	$5 \cdot 10^2$	$5 \cdot 10^3$	
Subcropping bedrock	0.5	0.15	$1 \cdot 10^3$	$2.5 \cdot 10^4$	$2 \cdot 10^2$	$3 \cdot 10^3$	
(b)							
Description	Friction angle [°]		Cohesion [N/m ³]		Unit weight [N/m ³]		
	Normal pdf		Normal pdf		Normal pdf		
	μ	σ	μ	σ	μ	σ	
Glacial deposits	32	3.2	4000	1500	20000	400	
Shallow glacial deposits	32	3.2	4000	1500	20000	400	
Glaciofluvial deposits	35	3.5	3000	1000	19000	350	
Fluvial deposits	36	3.6	0	0	19000	350	
Eluvial deposits	35	3.5	2500	800	19000	350	
Shallow eluvial deposits	35	3.5	2500	800	19000	350	
Landslide deposits	34	3.4	3500	1200	19000	350	
Landslide shallow deposits	34	3.4	3500	1200	19000	350	
Peat and bog	0	0	20000	6000	15000	200	
Eluvial deposits with high content of organic matter	0	0	20000	6000	15000	200	
Landslide deposits with boulders	38	3.8	1000	500	19000	350	
Landslide shallow deposits with boulders	38	3.8	1000	500	19000	350	
Subcropping bedrock	38	3.8	1000	500	19000	350	

K_s = saturated hydraulic conductivity

D_0 = maximum diffusivity

estimation as reported in Table 1. In lack of specific laboratory tests, hydraulic and mechanical soil properties were assigned to each deposit of the Quaternary deposits map from the literature, based on grain size distribution of the soil samples (hydraulic conductivity, Rawls et al. 1983; soil cohesion and friction angle, Harris 1977; Ho and Fredlund 1982; Phoon and Kulhawy 1999). Considering the assumed porosity of the deposits, the dimensionless coefficient C in Eq. 9 was set to the spatially uniform value of 0.38 (D’Odorico and Fagherazzi 2003). We did not insert excess rainfall and direct runoff in the analysis, since the expected high permeability and infiltration rate of the soil if compared to the modelled rainfall. Evapotranspiration was assumed to be negligible because of low temperatures and a high degree of cloud cover of the area during storms.

The soil parameter values were then calibrated by using the actual distribution of debris flows according to two criteria: 1) minimization of area classified as unstable without precipitation; 2) maximization of the number of debris flow source areas classified as unstable when the precipitation with 1,000 years return period is used (Fig. 4).

We used Monte Carlo simulations to treat the uncertainty in soil parameters and to calculate Pf. The input parameters were varied according to the assigned mean, standard deviation, and statistical distribution (Baecher and Christian 2003), shown in Table 1. Correlation matrices were introduced in the sampling of cohesion/friction angle values and hydraulic conductivity/diffusivity values. To reduce the number of simulations we used the Latin Hypercube sampling (McKay et al. 1979; Iman et al. 1981). In total 5,000 iterations are run for each rainfall scenario. The FoS was calculated at the maximum soil depth and at a time after the end of the storm, which corresponds to the peak of pressure head, T_{peak} . Since precipitations are longer than $T^* \approx 10$, T_{peak} was approximated as $T^*/20$ (Iverson 2000).

We validated the model by comparing the spatial distribution of landslides with the Pf calculated with 1,000 years return period precipitation. For the comparison, we considered only the upper part of the slide tracks (with a buffer of 10 m) and the shallow landslide

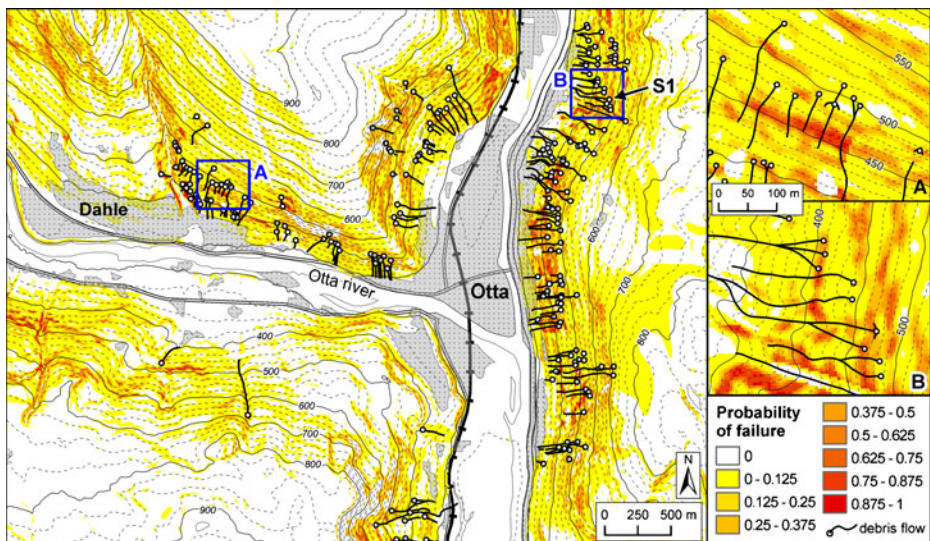
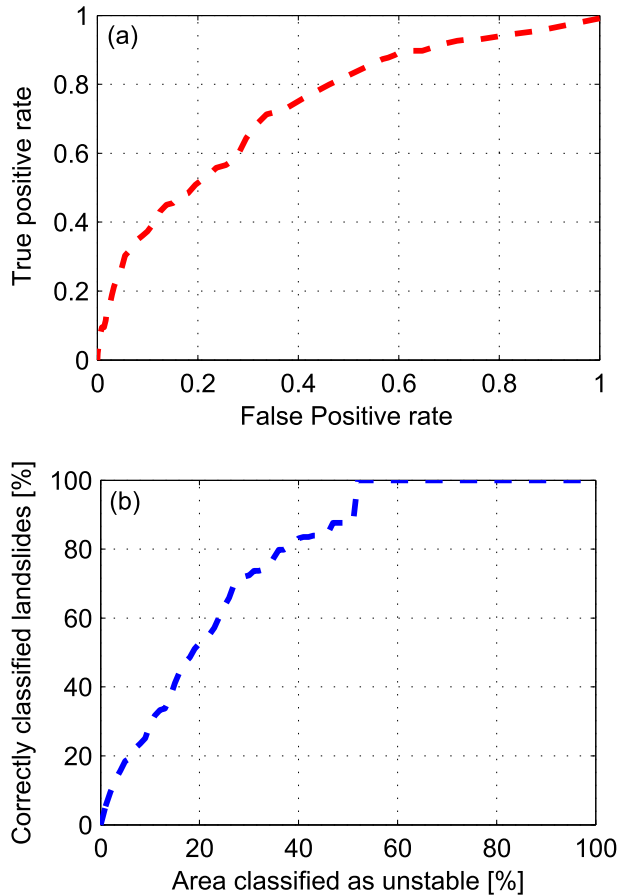


Fig. 4 Map of Pf for 1,000 years return period with no antecedent precipitation. The map also shows the landslide tracks and the buffer areas used in validation. The Pf for present and future scenarios is analysed in detail for the landslide area S1

Fig. 5 ROC curve (a) and success-rate curve (b) calculated on the map of Pf for 1,000 years return period with no antecedent precipitation



scarps (Fig. 4). ROC-curve and success rate curve (Chung and Fabbri 1999) were then calculated for the calibrated model (Fig. 5). Both curves show that the performance of the model is acceptable, especially considering that physically based models usually perform worse than models based on statistical methods or neural networks (Carrara et al. 2008; Godt et al. 2008).

4.3 Present and future instability conditions

The comparison between present and future stability conditions was done using all the 11 scenarios. In some figures we present results obtained using only the minimum and maximum precipitation variation, extracted for each return period (Table 2).

Differences between Pf at present and at future condition are shown in Fig. 6 for precipitation series with no antecedent precipitation and return periods of 5 years (Fig. 6a, b) and 1,000 years (Fig. 6c, d). The future scenario corresponds to the worst scenario selected among the 11 available models. The increment of Pf for the future scenario appears more pronounced in case of long return periods. Figure 7 shows a detail of Pf calculated with 50 years return period for the three precipitation series (i.e., no-filtered, filtered with 15 mm and 30 mm threshold in 4 days) and three scenarios (present, worst future scenario,

Table 2 Values of precipitations used in the analysis for different antecedent precipitation conditions and for different return periods

Antecedent precipitation	No			15 mm/4 days			30 mm/4 days		
	Present	Future		Present	Future		Present	Future	
Precipitation [mm/day]	Present	Min	Max	Present	Min	Max	Present	Min	Max
5 years	38	39	48	25	25	33	12	11	18
50 years	59	61	73	41	42	53	22	20	31
100 years	68	70	83	48	48	61	26	24	36
500 years	93	96	111	67	68	84	39	36	52
1000 years	106	108	125	78	79	96	46	43	60

best future scenario). The values of Pf change more due to the changes in antecedent precipitation (moving from left to right in Fig. 7) than to the different climate scenarios (moving from top to bottom in Fig. 7). That means that the variability of the possible

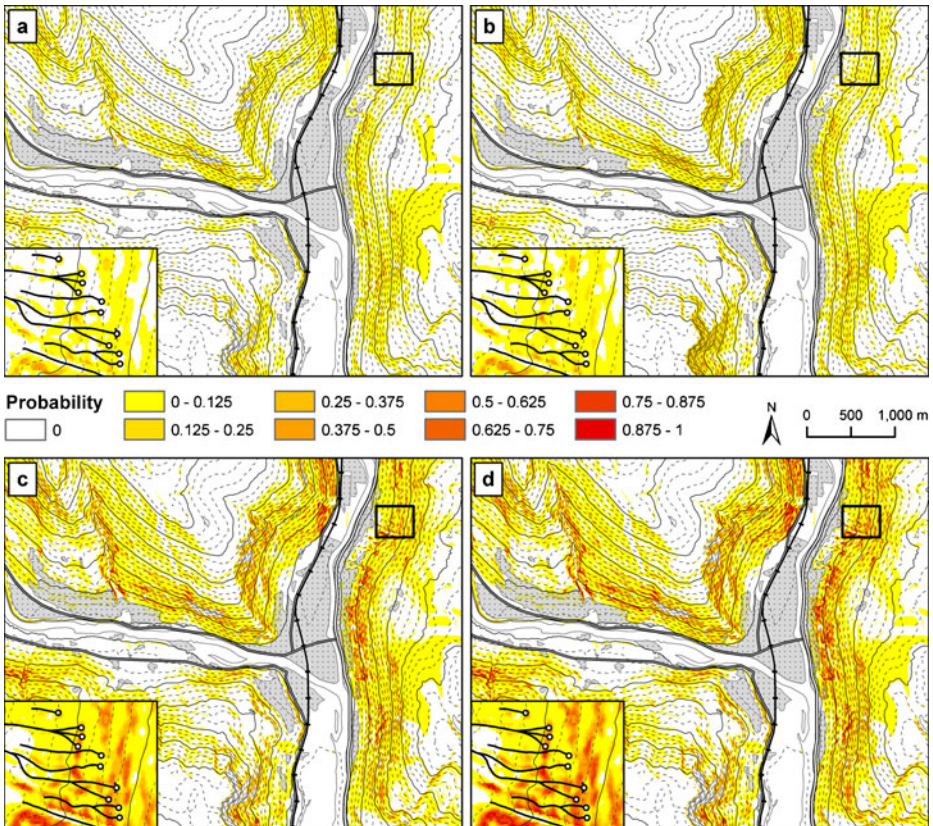


Fig. 6 Comparison between Pf at present and future condition (maximum variation). The maps show the case of no antecedent precipitation. Specifically, Pf for 5 years return period for present condition (a) and future condition (b); Pf for 1,000 years return period for present condition (c) and future condition (d). The boxes refer to the area B in Fig. 4

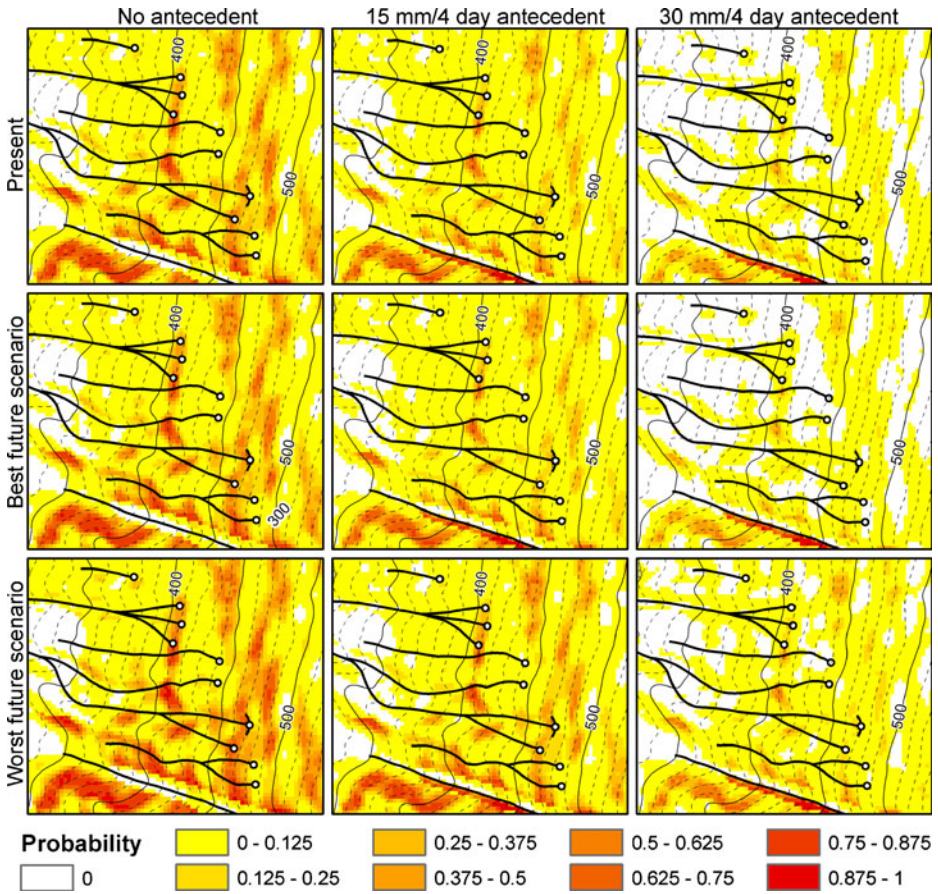


Fig. 7 Detail (quadrant B in Fig. 4) of Pf maps for 50 years return period. The figure shows the results obtained with three different antecedent precipitation conditions and three scenarios of extreme events

antecedent precipitation scenarios influences the variability of Pf more than the uncertainty in the modelling of the future precipitation conditions.

In order to quantitatively evaluate possible changes in stability conditions, we present two additional analyses for the entire study area and for selected landslide-prone areas.

For the entire study area, the percentage of unstable area above three thresholds of Pf (0.5, 0.25, 0.05), calculated with the three series of precipitation at present and future conditions, is shown in Fig. 8. The effect of antecedent precipitations is significant. Models without antecedent precipitation estimate an increase of unstable area for all the future scenarios, showing a unique trend (Fig. 8a, b, c). With antecedent precipitation of 15 mm in 4 days, some meteorological models predict a negligible increase of extreme events (e.g., 1%, see Table 2) and the stability conditions do not change (Fig. 8d, e, f). In case of antecedent precipitation of 30 mm in 4 days, we observe even a decrease of unstable areas, especially for extreme events with high return period (Fig. 8g, h, i).

Finally, we selected one landslide-prone area in glacial deposits (point S1 in Fig. 4), which represent the most susceptible materials in the area. Figure 9 compares the

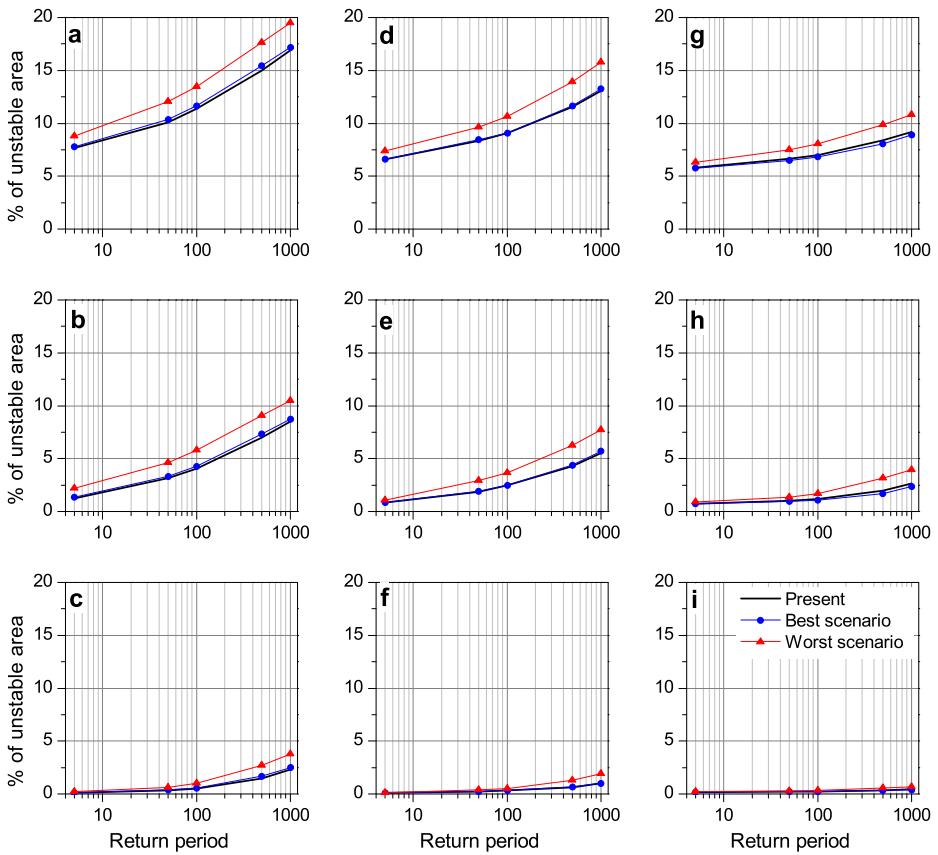


Fig. 8 Percentage of unstable area calculated with three thresholds of Pf for: no antecedent precipitation with $P_f \geq 0.05$ (a), $P_f \geq 0.25$ (b), $P_f \geq 0.5$ (c); 15 mm in 4 days antecedent precipitation with $P_f \geq 0.05$ (d), $P_f \geq 0.25$ (e), $P_f \geq 0.5$ (f); 30 mm in 4 days antecedent precipitation with $P_f \geq 0.05$ (g), $P_f \geq 0.25$ (h), $P_f \geq 0.5$ (i)

distributions of the Pf for present and future scenarios, derived by means of bootstrapping. We observe that the variability of the results increases with increasing antecedent precipitations. For example, considering the results with a return period of 1,000 years, we notice that future climate scenarios estimate increasing Pf for all the 11 scenarios in the case of no antecedent precipitation (Fig. 9c), whereas no changes and even decreasing Pf occur with antecedent precipitation (Fig. 9f, i). Similar results are obtained for landslide-prone areas in eluvial deposits.

4.4 Uncertainty and importance of variables

Global SA was performed using values of soil properties for eluvial and glacial deposits. The variable which increases the uncertainty the most is the depth of the soil both in case of glacial (Fig. 10a) and eluvial (Fig. 10b) deposits. Topographic data (i.e., contributing area, slope angle) also contribute to the uncertainty, followed by precipitation. Unexpectedly, soil cohesion, friction angle, hydraulic conductivity, and diffusivity are not the variables contributing the most to the final uncertainty of the model. This is an important result,

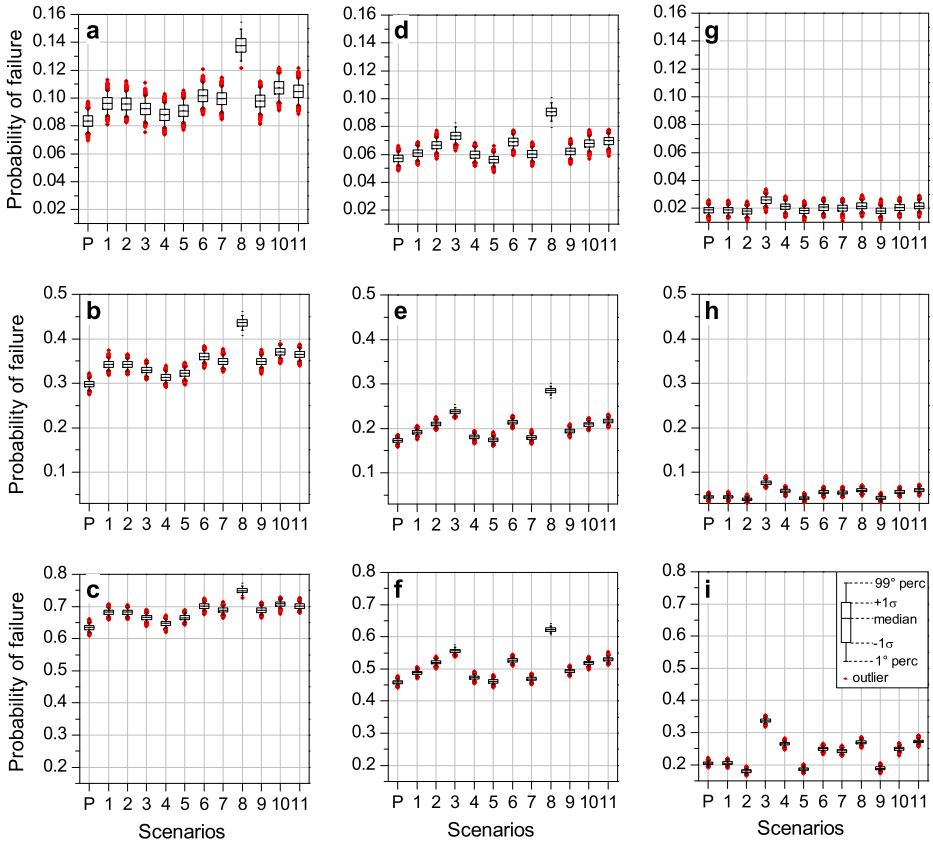


Fig. 9 Boxplots showing Pf distributions for present condition and the 11 scenarios for: no antecedent precipitation with a return period of 5 years (a), 100 years (b), and 1,000 years (c); 15 mm in 4 days antecedent precipitation with a return period of 5 years (d), 100 years (e), and 1,000 years (f); 30 mm in 4 days antecedent precipitation with a return period of 5 years (g), 100 years (h), and 1,000 years (i). Data are for the landslide S1 in Fig. 4

especially for the diffusivity, since this variable is highly uncertain and difficult to measure reliably.

The sensitivity plots are calculated on a subset extracted from the 5,000 Monte Carlo samples and from random locations. The baselines are chosen at the mean value of each variable. Antecedent precipitation is considered constant and set to 15 mm, as well as short and long precipitation duration set at 1 and 4 days, respectively. Figure 11 shows that slope angle is the most important variable in the model. Its influence on instability is clear when observing the pattern of Pf (Fig. 4), mainly influenced by slope angle values. Friction angle and cohesion also have great influence on FoS and show positive trends (i.e., increases of friction and cohesion result in increases of stability). The same order of importance is evident for the variable soil depth. This variable shows both positive and negative trends, meaning that increases of soil depth have complex effects on the values of FoS. This is due to the use of two hydrological models (i.e., long term and short term) coupled with the stability model. The variable soil depth affects FoS in different ways in the three models. The dominance of positive or negative trends depends on the values of other variables, as

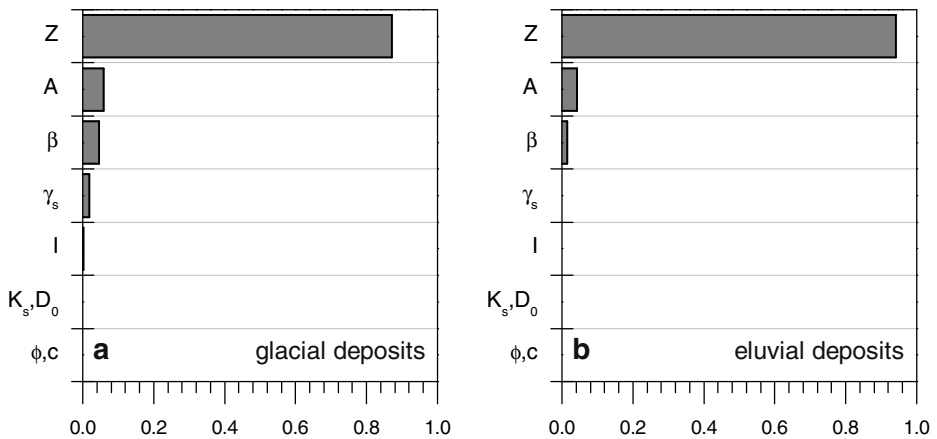


Fig. 10 Results of the global SA. The plots show the values of the first order index calculated for glacial (a) and eluvial (b) deposits

shown by the wide vertical spread at points in the sensitivity plot (Fig. 11c). Diffusivity also plays an important role but mainly at high values, whereas hydraulic conductivity, contributing area, soil unit weight and precipitation intensity have marginal importance. As expected, since the model is not additive, all variables show wide vertical spread at points.

5 Discussion

Physically-based models have been widely used to produce landslide susceptibility or hazard maps despite the relatively high uncertainty. Geological and hydrological conditions have high variability, which makes it difficult to spatially distribute soil properties and hydrological processes. Despite the uncertainty, these models provide estimations of relative changes in slope stability conditions due to variations in environmental settings (van Beek and van Asch 2004). Therefore, they are valuable tools in environmental planning and climate adaptation studies, once the uncertainty is assessed.

Uncertainty in our modelling arises from variations in global climate scenarios and epistemic uncertainty on hydrological and slope-stability model parameters.

The SA demonstrated that soil depth is the parameter that influences the model uncertainty the most and one of the variables that affects FoS values the most. Since soil depth controls the calculation of the steady-state lateral flow, the infiltration, and the stability, it affects the FoS values both positively and negatively (Fig. 11). The dominance of either positive or negative effect on FoS depends on the interactions with other variables (Fig. 11). For this reason, it is very important to perform local SA using methods that can account for interactions of inputs. The use of simple SA techniques, such as nominal range sensitivity (i.e., by individually varying only one of the inputs across its entire range, while holding the other inputs at their nominal value, Frey and Patil 2002), would generate misleading results. Since, the uncertainty of the models output is strongly controlled by soil depth (Fig. 10), future research should focus on a more reliable estimation of this variable.

Another result, apparently surprising, is the minor role of hydraulic conductivity and diffusivity in influencing the uncertainty and the values of FoS. This can be explained by the upper boundary of pressure head, physically limited at the beta-line (Iverson 2000), i.e.

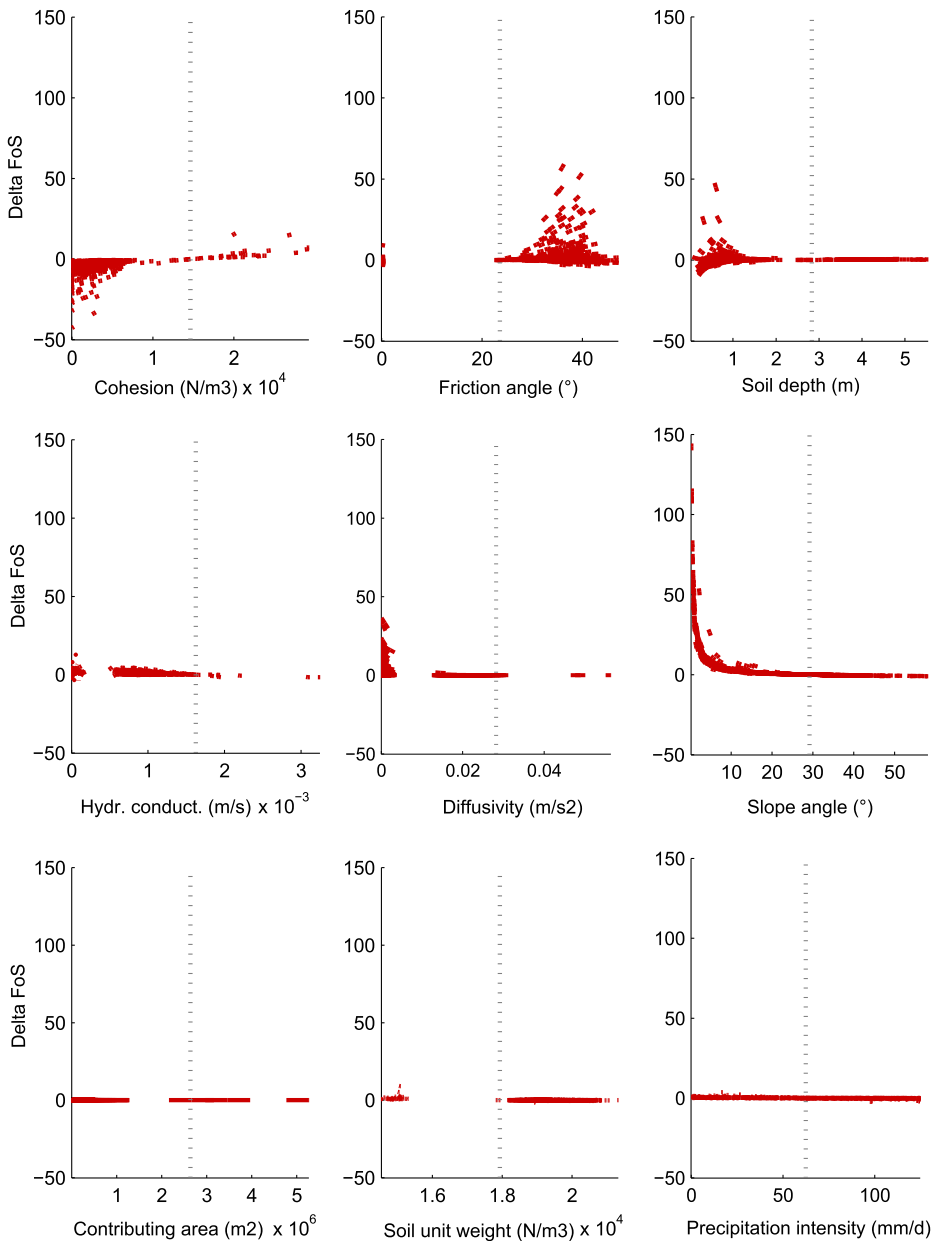


Fig. 11 Results of the graphical SA. The plots show the variation of the FoS (Delta FoS) due to variation of the variable from its baseline (mean value). The baseline is represented as dashed lines. The slope of the segments at each point of the plot represents the value of the partial derivative calculated at the point

$(Z, t) \leq Z \cos \beta$. Potentially extremely large variations of pressure head resulting from large variations in hydraulic conductivity and diffusivity are hampered by the beta-line correction. Moreover, hydraulic conductivity and diffusivity are positively correlated but have opposite effects on FoS, resulting in an overall small contribution on the variability of

the output. Again, interactions of variables are fundamental to understand the sensitivity of the output.

Cohesion and friction angle variables show significant positive effects on slope stability and interactions in the whole interval of variation. Slope angle and soil depth show negative effects but only in a small range of their interval of variation, meaning that small changes in slope angle and soil depth greatly control the calculation of FoS in not steep slopes and in not tick deposits.

The variability of global climatic scenarios influences the degree of confidence of the estimated changes in slope stability. When antecedent rainfalls are not considered, all future climate scenarios show a clear increase of precipitation (Fig. 3). This results in systematic decreases in slope stability, measured as variation in total unstable areas (Fig. 8) and in distribution of probability of failure (Fig. 9), for all future scenarios. At short return periods and at some scenarios, the changes are not significant due to the uncertainty in the modelling of the probability of failure, whereas at 1,000 years return period the trend is confirmed in all the scenarios (Fig. 9). Despite a clear trend at long return periods toward a decrease in slope stability, it is not possible to uniquely quantify the variation because of the uncertainty in future climate, which gives a wide range of possible slope stability conditions. When antecedent precipitations are introduced in the analysis, the uncertainty inherent to initial hydrological conditions of slopes is too high compared to climate variation. Changes in the total unstable areas are still modelled for the majority of the scenarios, but this variation is not statistically significant.

Our main finding is that the uncertainties in the predicted extreme precipitation events, hydrologic and slope stability modelling parameters, and antecedent precipitation conditions do not allow any accurate estimation of changes in stability conditions for shallow landslides. We were not able to identify a clear pattern in the changes of the stability conditions, apparently in contrast with literature (Dehn et al. 2000; Schmidt and Glade 2003; van Beek and van Asch 2004; Schmidt and Dikau 2004). Aside of the different environmental conditions (e.g., geology, climate) and modelling approaches (e.g., tank models versus distributed models, rainfall models versus coupled hydrological-stability models), which may lead to different results, we can recognize two main peculiarities in our approach.

First of all, we took the uncertainty in future climate prediction into consideration by using 11 climate scenarios. Even when not considering the uncertainty related to initial hydrological conditions (Fig. 9a, b, c), climate variability alone could be too high to recognize univocal trends. If we had used only one scenario, we would have concluded that slope stability conditions either do not change or significantly change for the scenario four or seven, respectively.

Secondly, we introduced a rough assessment of time scale by using several scenarios with different return periods. We could not investigate changes in landslide frequency due to intra-seasonal variations of precipitations (van Beek and van Asch 2004; Dehn et al. 2000; Stoffel et al. 2011).

This contribution focuses on the application of a physically based hydrological-stability model to study and understand the possible impact of precipitation changes in triggering shallow landslides. Although precipitation is the leading factor for slope instability in the study area, it is not possible to exclude variations of landslide frequency and intensity as a consequence of changes in temperature. For Mediterranean settings it was demonstrated that temperature increases could reduce landslide frequency by increasing evapotranspiration, which influences soil moisture before rainfall events (van Beek 2002). In alpine and sub-arctic environments, changes in temperature could affect snow accumulation and snow melting. Variations of snow melting can both directly influence landslide triggering and affect soil

moisture by reducing permafrost zones. The latter could shift areas affected by landslides toward higher elevations (Jomelli et al. 2004, 2007, 2009).

However, the effects of temperature changes have not been analysed in this paper, since our primary aim was to deeply investigate how changes in precipitation can affect landslide susceptibility.

6 Conclusions

By using a physically based hydrological-stability model we assessed the impact of the changes in precipitations on slope stability taking the uncertainty into consideration, which arises from both the variation of global climate scenarios and the epistemic uncertainty on hydrological and slope stability model parameters.

The use of 11 scenarios of future climate shows a wide range of variation for the projected climate and, as a consequence, changes in stability conditions due to climate change fall in a wide interval. Accounting for antecedent conditions further increases this uncertainty. We conclude that an accurate quantification of changes in stability conditions is not feasible, since the uncertainty in slope hydrologic and in slope stability conditions is higher than the climatic change.

Acknowledgments This work was realised within a post-doc scholarship, financially supported by the Norwegian Geological Survey (NGU) and the International Centre for Geohazards (ICG). We would like to thank Lars Harald Blikra, Kari Sletten, Knut Stalsberg and Asgeir Sorteberg for providing data and helpful suggestions. We are grateful to Giovanni B. Crosta for useful discussions about the analyses and the results. We would like to thank the three anonymous reviewers for the careful reading of the manuscript. Their comments have significantly improved the manuscript and the discussion. We really appreciate the help of Iain Henderson in reviewing the language.

References

- Alexandersson H, Førland EJ, Helminen J, Sjöblom N, Tveito OE (2001) Extreme value analysis in the Nordic countries. Norwegian Meteorological Institute, Oslo, Norway. Report 13/01 Klima
- Baecher GB, Christian JT (2003) Reliability and statistics in geotechnical engineering. Wiley, New York
- Bathurst JC, Moretti G, El-Hames A, Moaven-Hashemi A, Burton A (2005) Scenario modelling of basin-scale, shallow landslide sediment yield, Valsassina, Italian Southern Alps. *Nat Hazard Earth Syst Sci* 5:189–202
- Beven KJ, Kirkby MJ (1979) A physically base, variable contributing area model of basin hydrology. *Hydrolog Sci Bull* 24(1):43–69
- Borga M, Fontana GD, Cazorzi F (2002) Analysis of topographic and climatic control on rainfall-triggered shallow landsliding using a quasi-dynamic wetness index. *J Hydrol* 268(1–4):56–71
- Campbell RH (1974) Debris flows originating from soil slip during rainstorms in Southern California. *Q J Eng Geol Hydrol* 7(4):339–449
- Carrara A, Crosta G, Frattini P (2008) Comparing models of debris-flow susceptibility in the alpine environment. *Geomorphology* 94(3–4):353–378
- Casadei M, Dietrich WE, Miller NL (2003) Testing a model for prediction of the timing and location for shallow landslide initiation in soul-mantled landscape. *Earth Surf Process Landforms* 28:925–950
- Chung CF, Fabbri AG (1999) Probabilistic prediction models for landslide hazard mapping. *Photogramm Eng Remote Sens* 65(12):1389–1399
- Collison A, Wade S, Griffiths J, Dehn M (2000) Modelling the impact of predicted climate change on landslide frequency and magnitude in SE England. *Eng Geol* 55:205–218
- Crosta GB (1998) Regionalization of rainfall thresholds: an aid to landslide hazard evaluation. *Environ Geol* 35(2–3):131–145

- Crosta GB, Frattini P (2001) Rainfall thresholds for triggering soil slips and debris flow. In: Proceedings of EGS 2nd Plinius Conference 2000, Mediterranean Storms, Siena: 463–488
- Crosta GB, Frattini P (2008) Rainfall-induced landslides and debris flows. *Hydrolog Process* 22:473–477
- Cruden DM, Varnes DJ (1996) Landslides types and processes. In: Turner AK, Schuster RL (eds) *Landslides: investigation and mitigation*. Transportation Research Board Special Report 247. National Academy Press, WA, 36–75
- Davison A, Hinkley D (1997) *Bootstrap methods and their application*. Cambridge University Press, Cambridge
- Dehn M (1999) Application of an analog downscaling technique to the assessment of future landslide activity—a case study in the Italian Alps. *Clim Res* 13(2):103–113
- Dehn M, Buma J (1999) Modelling future landslide activity based on general circulation models. *Geomorphology* 30:175–187
- Dehn M, Burger G, Buma J, Gasparetto P (2000) Impact of climate change on slope stability using expanded downscaling. *Eng Geol* 55:193–204
- Dikau R, Schrott L (1999) The temporal stability and activity of landslides in Europe with respect to climatic change (TESLEC): main objectives and results. *Geomorphology* 30:1–12
- Dixon N, Brook E (2007) Impact of predicted climate change on landslide reactivation: case study of Mam Tor, UK. *Landslides* 4:137–147
- D’Odorico P, Fagherazzi S (2003) A probabilistic model of rainfall-triggered shallow landslides in hollow: a long-term analysis. *Water Resour Res* 39(9):1262–1275
- D’Odorico P, Fagherazzi S, Rigon R (2005) Potential for landsliding: dependence on hypsograph characteristics. *J Geophys Res* 110(F1):F01007
- Flageollet JC, Maquaire O, Martin B, Weber D (1999) Landslides and climatic conditions in the Barcelonnette and Vars basins (Southern French Alps, France). *Geomorphology* 30:65–78
- Førland EJ (1987) Beregning av ekstrem nedbor (Estimation of extreme precipitation). Norwegian Meteorological Institute, Oslo, Norway. DNMI report 23/87 Klima. In Norwegian
- Førland EJ, Kristoffersen D (1989) Estimation of extreme precipitation in Norway. *Nord Hydrol* 20:257–276
- Frattini P, Crosta G, Sosio R (2009) Approaches for defining thresholds and return periods for rainfall-triggered shallow landslides. *Hydrolog Process* 23(10):1444–1460
- Frey HC, Patil SR (2002) Identification and review of sensitivity analysis methods. *Risk Anal* 22(3):553–578
- Glade T (2000) Modelling landslide-triggering rainfalls in different regions in New Zealand—the soil water status mode. *Z Geomorphol* 122:63–84
- Godt JW, Baum RL, Savage WZ, Salciarini D, Schulz WH, Harp EL (2008) Transient deterministic shallow landslide modeling: requirements for susceptibility and hazard assessments in a GIS framework. *Eng Geol* 102(3–4):214–226
- Guzzetti F, Peruccacci S, Rossi M, Stark CP (2007) Rainfall thresholds for the initiation of landslides in central and southern Europe. *Meteorol Atmos Phys* 98(3–4):239–267
- Harris C (1977) Engineering properties, groundwater conditions, and the nature of soil movement on a solifluction slope in North Norway. *Q J Eng Geol Hydrogeol* 10:27–43
- Ho DYF, Fredlund DG (1982) A multi-stage triaxial test for unsaturated soils. *Geotech Test J* 5:18–25
- Homma T, Saltelli A (1996) Importance measures in global sensitivity analysis for nonlinear models. *Reliab Eng Syst Saf* 52:1–17
- Iman RL, Helton JC, Campbell JE (1981) An approach to sensitivity analysis of computer models, Part I. Introduction, input variable selection and preliminary variable assessment. *J Qual Technol* 13(3):174–183
- Iverson RM (2000) Landslide triggering by rain infiltration. *Water Resour Res* 36:1897–1910
- Jacques J, Lavergne C, Devictor N (2006) Sensitivity analysis in presence of model uncertainty and correlated input. *Reliab Eng Syst Saf* 91(10–11):1126–1134
- Jaedicke C, Solheim A, Blikra LH, Stalsberg K, Sorteberg A, Aaheim A, Kronholm K, Vikhamar-Schuler D, Isaksen K, Sletten K, Kristensen K, Barstad I, Melchiorre C, Høydal ØA, Mestl H (2008) Spatial and temporal variations of Norwegian geohazards in a changing climate, the GeoExtreme project. *Nat Hazards Earth Syst Sci* 8:893–904
- Jomelli V, Pech VP, Chochillon C, Brunstein D (2004) Geomorphic variations of debris flows and recent climatic change in the French Alps. *Clim Chang* 64:77–102
- Jomelli V, Brunstein D, Grancher D, Pech P (2007) Is the response of hill slope debris flows to recent climate change univocal? A case study in the Massif des Ecrins (French Alps). *Clim Chang* 85:119–137
- Jomelli V, Brunstein D, Déqué M, Vrac M, Grancher D (2009) Impacts of future climatic change (2070–2099) on the potential occurrence of debris flows: a case study in the Massif des Ecrins (French Alps). *Clim Chang* 97:171–191
- McKay MD, Conover WJ, Beckman RJ (1979) Comparison of three methods for selecting values of input variables in the analysis of output from a computer code. *Technometrics* 21:239–245

- Montgomery DR, Dietrich WE (1994) A physically based model for the topographic control on shallow landsliding. *Water Resour Res* 30:1153–1171
- Nakicenovic N, Alcamo J, Davis G, de Vries B, Fenhann J, Gaffin S, Gregory K, Grübler A, Jung TY, Kram T, Lebre La Rovere E, Michaelis L, Mori S, Morita T, Pepper W, Pitcher H, Price L, Riahi K, Roehrl A, Rogner H, Sankovski A, Schlesinger M, Shukla P, Smith S, Swart R, van Rooijen S, Victor N, Dadi Z (2000) Special report on emission scenarios: a special report of working group III of the Intergovernmental Panel on Climate Change. University Press, Cambridge
- NERC (1975) Flood studies report, vol. II. Meteorological studies. National Environment Research Council, London
- Phoon KK, Kulhawy FH (1999) Characterization of geotechnical variability. *Can Geotech J* 36:612–624
- Plate T, Bert J, Band P (2000) Visualizing the function computed by a feed-forward neural network. *Neural Comput* 12(6):1337–1354
- Rawls WJ, Brakensiek DL, Miller N (1983) Green-Amp infiltration parameters from soil data. *J Hydraul Eng* 109:62–70
- Rebetez M, Lugon R, Baeriswyl PA (1997) Climatic change and debris flows in high mountain regions: the case of the Ritigraben torrent (Swiss Alps). *Clim Change* 36:371–389
- Rosso R, Rulli MC, Vannucchi G (2006) A physically based model for the hydrologic control on shallow landsliding. *Water Resour Res* 42:W06410
- Saltelli A (2002) Sensitivity analysis for importance assessment. *Risk Anal* 22(3):579–590
- Sandersen F, Bakkehoi S, Hesten E, Lied K (1996) The influence of meteorological factors on the initiation of debris-flows, rockfalls, rockslides and rockmass stability. *Landslide. Proceeding of the seventh international symposium on landslides, June 1996, Trondheim. A.A. Balkema, Rotterdam*
- Schmidt J, Dikau R (2004) Modeling historical climate variability and slope stability. *Geomorphology* 60:433–447
- Schmidt M, Glade T (2003) Linking global circulation model outputs to regional geomorphic models: a case study of landslide activity in New Zealand. *Clim Res* 25(2):135–150
- Simoni S, Fabrizio Z, Giacomo B, Riccardo R (2008) Modelling the probability of occurrence of shallow landslides and channelized debris flows using GEOtop-FS. *Hydrolog Process* 22(4):532
- Skempton AW, De Lory FA (1957) Stability of natural slopes in London Clay. In: *Proceedings of the 4th International Conference on Soil Mechanics and Foundation Engineering 2, London*
- Sletten K, Blikra LH (2007) Holocene colluvial (debris-flow and water-flow) processes in eastern Norway: stratigraphy, chronology and palaeoenvironmental implications. *J Quaternary Sci* 22:619–635
- Sobol IM (1993) Sensitivity estimates for nonlinear mathematical models. *Math Model Comput Exp* 1:407–414
- Solomon S, Qin D, Manning M, Chen Z, Marquis M, Averyt KB, Tignor M, Miller HL (2007) *Climate change 2007: the physical science basis*. Cambridge University Press, Cambridge
- Sorteberg A, Andersen MS (2008) Regional precipitation and temperature changes for Norway 2011 and 2026. Results from 11 simulations using 8 European regional models. Report Series of the Bjerknes Centre for Climate Research. BCCR Report No 28
- Stoffel M, Bollschweiler M, Beniston M (2011) Rainfall characteristics for periglacial debris flows in the Swiss Alps: past incidences–potential future evolutions. *Clim Change* 105(1–2):263–280
- Tarboton DG (1997) A new method for the determination of flow direction and upslope areas in grid digital elevation models. *Water Resour Res* 33:309–319
- Terlien MTJ (1998) The determination of statistical and deterministic hydrological landslide-triggering thresholds. *Environ Geol* 35(2–3):124–130
- van Beek R (2002) Assessment of the influence of changes in land use and climate on landslide activity in a Mediterranean environment. *Netherlands Geographical Studies* 294, Utrecht, The Netherlands
- van Beek LPH, van Asch TWJ (2004) Regional assessment of the effects of land-use change on landslide hazard by means of physically based modelling. *Nat Hazards* 31(1):289–304
- Wieczorek GF, Glade T (2005) Climatic factors influencing occurrence of debris-flows. In: Jacob M, Hungr O (eds) *Debris-flow hazard and related phenomena*. Springer, Berlin, pp 325–362
- Wilkinson PL, Anderson MG, Lloyd D (2002) An integrated hydrological model for rain-induced landslide prediction. *Earth Surf Proc Land* 27:1285–1297
- Wilson RC, Wieczorek GF (1995) Rainfall thresholds for the initiation of debris flows at La Honda, California. *Environ Eng Geosci* 1(1):11–27